

Learning Dynamic Graph Embeddings for Accurate Detection of Cognitive State Changes in Functional Brain Networks

Yi Lin ¹, Jia Hou ^{1,2}, Defu Yang ^{1,2}, Chengang Yan ², Minjeong Kim ³, Paul J Laurienti ⁴ and Guorong Wu ^{1,5}

¹ Department of Psychiatry, University of North Carolina at Chapel Hill, Chapel Hill, NC, USA

² School of Automation, Hangzhou Dianzi University, Hangzhou, Zhejiang, China

³ Department of Computer Science, University of North Carolina at Greensboro, Greensboro, NC, USA

⁴ Department of Radiology, Wake Forest School of Medicine, Winston Salem, NC, USA

⁵ Department of Computer Science, University of North Carolina at Chapel Hill, Chapel Hill, NC, USA

Abstract. Mounting evidence shows that brain functions and cognitive states are dynamically changing even in the resting state rather than remaining at a single constant state. Due to the relatively small changes in BOLD (blood-oxygen-level-dependent) signals across tasks, it is difficult to detect the change of cognitive status without requiring prior knowledge of the experimental design. To address this challenge, we present a dynamic graph learning approach to generate an ensemble of subject-specific *dynamic graph embeddings*, which allows us to use brain networks to disentangle cognitive events more accurately than using raw BOLD signals. The backbone of our method is essentially a representation learning process for projecting BOLD signals into a latent vertex-temporal domain with the greater biological underpinning of brain activities. Specifically, the learned representation domain is jointly formed by (1) a set of harmonic waves that govern the topology of whole-brain functional connectivities and (2) a set of Fourier bases that characterize the temporal dynamics of functional changes. In this regard, our *dynamic graph embeddings* provide a new methodology to investigate how these self-organized functional fluctuation patterns oscillate along with the evolving cognitive status. We have evaluated our proposed method on both simulated data and working memory task-based fMRI datasets, where our dynamic graph embeddings achieve higher accuracy in detecting multiple cognitive states than other state-of-the-art methods.

Keywords: Graph learning, functional brain networks, change detection.

1 Introduction

The human brain is a complex, interacting network with unique topological properties ([Sporns et al., 2004](#)). Advances in network neuroscience have aroused much interest in understanding how distinct brain regions work together to maintain high-level brain functions and behaviors. To that end, the notion of functional connectivity (FC) comes to the stage to characterize the functional relationship between spatially separated anatomical brain regions, which can be measured, yet indirectly, either through the electrical activities in the

electroencephalogram (EEG) ([Stam et al., 2007](#)) or from the blood-oxygen-level-dependent (BOLD) signals in functional magnetic resonance imaging (fMRI) ([Biswal et al., 1995](#)).

FC is essentially a statistical measurement that reflects the synchronization degree of fluctuation patterns between two brain regions with whole-brain connectivity analyses allowing for the examination of network topology ([Rubinov and Sporns, 2010](#); [Sporns, 2011](#)).

Tremendous strides have been made in functional brain networks by assuming FC remains stationary throughout the entire scan session ([Bastos and Schoffelen, 2016](#); [Friston, 2011](#); [Van Den Heuvel and Pol, 2010](#)), which is often known as static FC. However, mounting studies have revealed that the functional brain networks change dynamically over time and manifest as multiple brain states even in the resting state, implying that static FC may not capture the full extent of dynamic brain networks ([Hutchison et al., 2013](#)). Thus, research interest is shifting towards quantifying dynamic changes in FC (aka. dynamic FC), which may provide greater insight into the fundamental properties of brain networks ([Allen et al., 2018](#); [Gonzalez-Castillo and Bandettini, 2018](#); [Shine et al., 2015](#)). In the past decade, a lot of computational methods have been developed to characterize functional dynamics, which can be roughly categorized into two groups: (1) statistical modeling for detecting temporal change points ([Cribben et al., 2012](#); [Xu and Lindquist, 2015](#)) and (2) the sliding window technique ([Allen et al., 2014](#); [Calhoun et al., 2014](#); [Damaraju et al., 2014](#); [Rashid et al., 2014](#)).

Regarding statistical modeling on functional dynamics, the key is to identify significant changes in the network structure, which presumably underlies cognition changes. For example, Cribben *et al.* ([Cribben et al., 2012](#)) proposed a dynamic connectivity regression (DCR) method to detect temporal changing points, which first partitions the time course into intervals and then estimates connectivity networks within each interval using the statistical inference model learned from population data. After that, the classic DCR method has been improved in ([Xu and Lindquist, 2015](#)) by utilizing a sparse matrix estimation technique and a hypothesis testing procedure to detect changing points. Besides recognizing the changing positions in the signal domain, a novel statistical inference method ([Schröder and Ombao, 2019](#)) has been recently proposed to identify frequency-specific changes using a cumulative sum-type test statistic, that is devised to detect subtle disruptions in normal brain functioning that precede the onset of an epileptic seizure. Although statistical inference provides a potentially powerful method for tracking dynamic FC, the intensive computational cost limits its application only to small-scale networks.

A more common and computationally effective way to understand dynamic FC is the sliding window technique ([Allen et al., 2014](#); [Calhoun et al., 2014](#); [Damaraju et al., 2014](#); [Rashid et al., 2014](#)). In general, the entire time course of BOLD signals is first partitioned into a set of (overlapping or non-overlapping) sliding windows. Given that brain function stays stationary within a short time window, the topology changes of functional brain networks across the sliding windows are supposed to underline the intrinsic functional dynamics. In light of this, clustering the within-sliding-window FC matrices is often used to identify the change of cognitive states.

However, the sliding window approach is very sensitive to the window size and BOLD signal noise, resulting in less replicable results ([Hindriks et al., 2016](#); [Shakil et al., 2016](#)).

Due to the low signal-to-noise ratio and high spatial-temporal redundancy in BOLD signals ([Krüger and Glover, 2001](#)), the correlation between BOLD signals and the intrinsic changing points is often not strong enough to yield reliable tracking of cognitive states. To illustrate this, we randomly select two regions (left parietal cortex and right prefrontal cortex) and calculate the central temporal difference of the BOLD time course, as shown by the red dash curves at the top of **Fig. 1**. For clarity, we only plot the magnitude of the central temporal difference and overlay with green delta peaks, which designate the pre-defined switch points of tasks in a multi-task fMRI scan. It is apparent that the peaks of the curve (red peak points) have significant offsets compared to the ground truth, which will undermine the accuracy of detecting state changes. Furthermore, we average the whole-brain BOLD signal trajectories and then show the central temporal difference (solid red curve) of the average BOLD time course in the grey box of **Fig. 1**. The correlation ($r = -0.09$) between the ground truth and whole-brain average of the BOLD signals not only shows a negative relationship but also indicates a significant gap between the two data domains. Since the sliding window technique is widely used to capture functional dynamics, we examine the network difference across sliding windows. The curve of network difference between two neighboring sliding windows is displayed in the purple box of **Fig. 1**, where we use Gromov-Hausdorff distance ([Lee et al., 2012](#)) to measure the topology difference between two functional brain networks. Again, the temporal changes of network topologies do not closely synchronize with the transition of

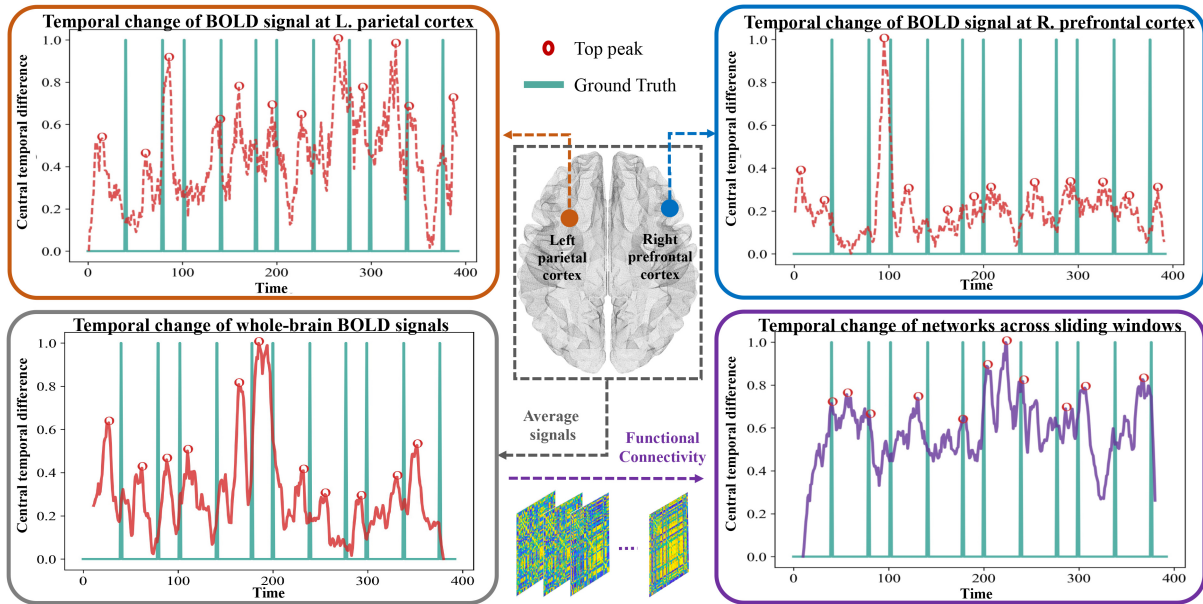


Fig. 1. The temporal patterns (measured by the magnitude of central difference) in BOLD signals often have a weak correlation with the task demand changes (green delta peaks) either using the regional BOLD time course (red and blue boxes) or whole-brain average BOLD signals (grey box). Likewise, the temporal change of network topology difference across sliding windows does not synchronize closely to the changes in task demands (purple box).

cognitive states. Thus, multiple threads of evidence clearly show a need to derive a better feature representation from the BOLD signals where the evolution of the new data representation synchronizes with the intrinsic cognitive state changes associated with changes in task demands.

To address this challenge, we introduce a new dynamic graph learning approach to generate new feature representations from the BOLD signals that have an enhanced correlation with the real cognitive changes and thus yield more accurate cognitive change detection results. The workflow of our learning approach is shown in **Fig. 2(a)**. In general, our method opts to project BOLD time courses into a latent vertex-time domain (displayed in the red box), where the projection coefficients constitute the new feature representations for detecting cognitive changes by the classic temporal clustering method. The backbone of our approach is the latent vertex-time domain, which allows us to capture the dynamic patterns supported by the subject-specific intrinsic network topology. Since the brain network is often encoded in a graph structure, we regard the array of the BOLD signals at each time point (represented as columns in the gray box in **Fig. 2(b)**) as a graph signal, where the element-to-element relationship in the data array is regulated by the corresponding node-to-node connectivity degree in the graph.

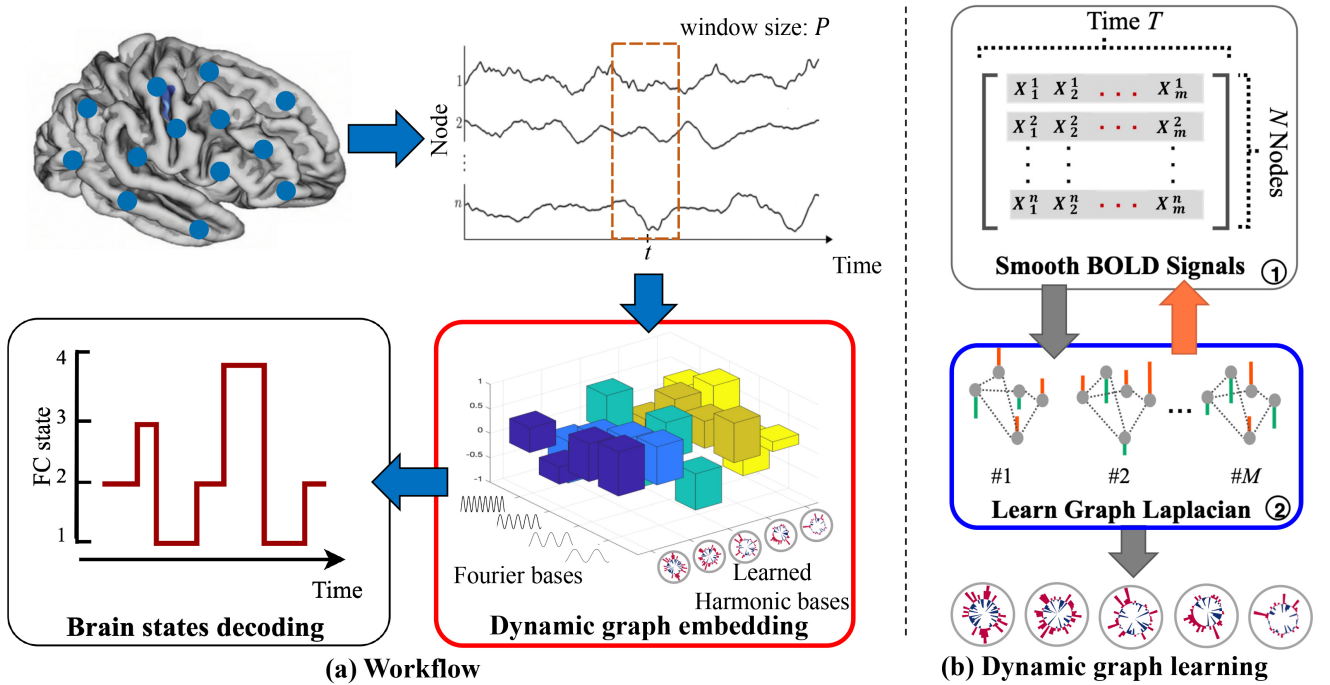


Fig. 2. The overall pipeline of our proposed method: (a) the workflow and (b) learning harmonic bases by utilizing the dynamic graph learning approach.

In this context, we conceptualize the BOLD time courses as an evolving graph signal (illustrated in the blue box of **Fig. 2(b)**), which forms a dynamic system. In control theory, it is well studied that the dynamics of the system are governed by the Eigen-system of Laplacian operator ([Gu et al., 2015](#); [Honey et al., 2009](#); [Medaglia et al., 2017](#)). To that end, we first extend our previous work ([Kim et al., 2019](#)) from learning graph Laplacian to the new paradigm of learning the dynamic graph Laplacian of the vertex-time domain. Indeed, we have the closed-form solution to derive the joint Eigen-system of the learned dynamic graph Laplacian, which consists

of (1) a set of harmonic waves (bases) for characterizing the network topology and (2) a set of Fourier bases for capturing dynamic changes. After that, we construct the dynamic graph embeddings for each sliding window by projecting the BOLD signals through the joint harmonic-Fourier bases. Finally, we employ an off-the-shelf temporal clustering method ([Ng et al., 2002](#)) to detect changing positions based on the dynamic graph embeddings. We evaluate the power of our dynamic graph embedding method on both simulated data and task-based fMRI data involving working memory, where we have achieved more accurate detection results than using raw BOLD data.

2 Materials and methods

2.1 Data description

Simulate data. First, SimTB toolbox ([Erhardt et al., 2012](#)) is employed to create simulated fMRI time series with K brain states, where $K = 3$ in our simulated experiments. **Fig. 3** (top) shows three FC matrices at the pre-defined cognition stages, where each FC matrix consists of three modules (communities) along the diagonal line. For each possible pair of nodes with the same module, the connectivity degree is set to one. No cross-module connectivity is allowed (equals to zero). Here, we set two changes of FC at $t = 100$ and $t = 200$ (in seconds), respectively. Therefore, each brain state could last 100 seconds. Based on this setting, we use SimTB to generate the simulated dynamic fMRI data with a total length of 300 TRs (shown at the bottom of **Fig. 3**). We repeat this process 100 times and evaluate the sensitivity of our proposed dynamic graph learning method with respect to window size, noise level, and network size (number of nodes) based on the 100 simulated fMRI dataset as follows. We evaluate our proposed change detection method on simulated data in Section 3.1.

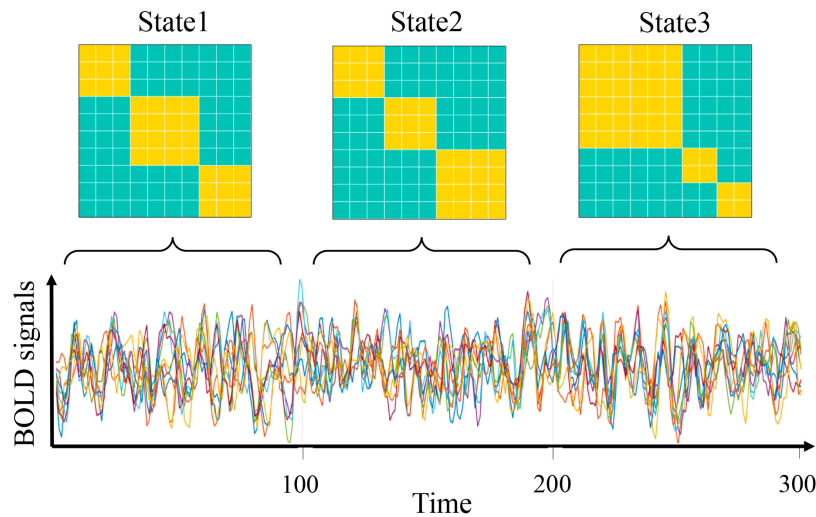


Fig. 3. Top: 3 simulated brain states with 10 brain regions are simulated (each with 3 modules of different dimension where the size of the modules in each state are defined as state1: [3×3, 4×4, 3×3], state2: [3×3, 3×3, 4×4], and state3: [6×6, 2×2, 2×2]). Bottom: Given the simulated brain states, simulated fMRI data with 2 changes of FC at $t = 100$ and $t = 200$ can be generated by SimTB toolbox.

Real data. We used working memory fMRI data from 60 healthy subjects selected from the Human Connectome Project ([Van Essen et al., 2013](#)). The working memory tasks in each fMRI scan include 2-back and 0-back task events of body parts, places, faces, and tools, as well as resting fixation periods. The BOLD-contrast images in echo-planar imaging sequence were collected using a 3T ConnectomeScanner adapted from a Siemens Skyra (acquisition time = 5 min and 1 s, TR= 0.72 s, TE = 33 ms, 2mm isotropic resolution). We used the minimally preprocessed data ([Glasser et al., 2013](#)) and additionally performed the following preprocessing steps. First, motion correction was performed using AROMA ([Pruim et al., 2015](#)). The data were then bandpass filtered (0.009-0.8 Hz) and a regression was performed to removed whole-brain gray matter, white matter, and cerebrospinal fluid signal as well as realignment parameters and the first temporal derivative. Data were then parcellated into 268 regions by the Shen 268 brain region atlas ([Shen et al., 2013](#)), and new time courses were generated by averaging the signal of all voxels in each region. We first focused on 58 brain regions, which are located at the default mode network (DMN) and attention network (ATN) since they are closely related to the resting periods and working memory task, respectively (see Supplementary Material for list of atlas regions). Then, we demonstrated the scalability of our method using all brain regions. In Section 3.2, we evaluated the performance of our proposed method on detecting changes of functional connectivity and the discriminative power of our proposed method in recognizing different functional tasks on real fMRI data involving the working memory task.

2.2 Construction of joint vertex-time domain

Any brain network can be described as a graph structure $G = (V, E, W)$, where a set of N brain regions consists of the node-set V . E denotes the edge-set, where the connectivity degrees are encoded into an adjacent matrix $W = [w_{ij}]_{i,j=1}^N$. In fMRI, each element w_{ij} ($-1 \leq w_{ij} \leq 1$) is essentially the statistical correlation of BOLD signals between the regions V_i and V_j . Given the adjacency matrix W , the underlying Laplacian matrix can be calculated as $L_G = D - W$, where D is a diagonal matrix defined as $D_{ii} = \sum_{j=1}^N w_{ij}$. Supposed the BOLD time course has T sampled time points. We use data matrix $X = [x_t]_{t=1,\dots,T} \in R^{N \times T}$ to represent the entire brain BOLD time series, where $x_t \in R^N$ is a column vector denoting the “snapshot” of the whole-brain BOLD signals at a particular time t .

In order to capture the putative spatio-temporal patterns from BOLD signals, we opt to find a hidden domain, called joint vertex-time domain, which allows us to disentangle the mixed spatial-temporal information in BOLD signals into the topological patterns (characterizing intrinsic functional connectivities in the brain) and dynamic patterns (characterizing functional dynamics). To be more specific, this domain is formed by (1) a set of Fourier bases Φ_T for characterizing the dynamic fluctuation pattern in the temporal domain and (2) a set of harmonic bases Φ_G for representing the topological property of the functional brain network in the graph spectrum domain. Since the Eigen-system of the Laplacian operator controls the dynamic characteristics of time-varying FC, we can arrive at the solution of the Fourier bases and harmonic bases by finding the joint Laplacian matrix from the temporal and graph spectrum domains as follows.

First, we introduce the standard definition of the dynamic Laplacian matrix in the temporal domain. The first-order difference operator in the temporal domain is defined as:

$$X\nabla_T = x_t - x_{t-1} \quad (1)$$

with periodic boundary conditions (i.e., $x_{T+1} = x_1$), and the second-order temporal derivative is defined as:

$$XL_T|_t = 2x_t - x_{t-1} - x_{t+1} \quad (2)$$

where the dynamic Laplacian matrix is denoted by:

$$L_T = \nabla_T^\top \nabla_T \in R^{N \times N} \quad (3)$$

Since L_T is fixed and circulant ($x_{T+1} = x_1$), the dynamic Laplacian L_T which encodes Eigen-system of the temporal domain can be decomposed into $L_T = \Phi_T \Lambda_T \Phi_T^\top$, where Eigenvectors Φ_T and the diagonal Eigenvalue matrix Λ_T have the closed-form solution as:

$$\Phi_T(t, k) = \left[\frac{e^{-j\left(\frac{2\pi(k-1)}{T}\right)}}{\sqrt{T}} \right]_{t,k=1,\dots,T} \quad (4)$$

$$\Lambda_T(t, t) = \lambda_T(t) = 2(1 - \cos(\frac{2\pi(t-1)}{T})) \quad (5)$$

It is clear that the Eigenvectors Φ_T in Eq. (4) is essentially a set of Fourier waves with the temporal frequency being defined in Eq. (5).

Second, in the graph spectrum domain, the network-specific harmonic bases Φ_G can be obtained by applying singular vector decomposition (SVD) ([Cline and Dhillon, 2006](#)) on the latent graph Laplacian L_G of the underlying brain network, i.e., $L_G = \Phi_G^\top \Lambda_G \Phi_G$, where Φ_G and Λ_G are Eigenvectors and Eigenvalues, respectively. Although it is straightforward to calculate the graph Laplacian matrix L_G from the adjacency matrix W , we propose to optimize L_G from BOLD signals for the following reasons. (1) The possible external noise in BOLD signals might undermine the accuracy of signal correlations in the adjacency matrix ([Kim et al., 2019](#)). (2) Since the calculation of adjacency matrix W is based on the entire BOLD signals, it has limited power to capture the functional fluctuations of BOLD signals running in the joint vertex-time domain. In light of this, we opt to learn the dynamic graph Laplacian matrix L_G , by following the learning process described below.

2.3 Learning dynamic graph Laplacian from BOLD signals

To estimate an intrinsic graph Laplacian that encodes the topology of the dynamic functional network, we extend our previous work ([Kim et al., 2019](#)) to learn a dynamic graph Laplacian L_G in the vertex-time domain instead of learning graph Laplacian only in the vertex domain. As shown in **Fig.2 (b)**, we propose to jointly de-noise the observed signals X and discover the dynamic graph Laplacian matrix L_G from the latent clean BOLD signals.

First, we propose to estimate L_G based on the intrinsic BOLD signals Y instead of observed signals X . Generally, Y should be close to the observed X , which is constrained by a ℓ_2 -norm data fitting term $\| X - Y \|_F^2$

to measure the distance between X and Y . Given the intrinsic BOLD signals Y , we estimate the network graph Laplacian L_G by introducing the following three constraints to guarantee a well-posed objective function.

(1) Temporal smoothness constraint on Y . Since the BOLD signals have been smoothed by bandpass filters (e.g., 0.009-0.8 Hz), it is reasonable to assume that the BOLD signal changes relatively slowly over short periods of time. Thus we require the time series of a BOLD signal at each brain region (each row of Y) should be smooth between y_t^i and y_{t+1}^i :

$$\| Y \|_{L_T} = \text{tr}(Y^\top L_T Y) = \sum_{i=1}^N \sum_{t=1}^T (y_{t+1}^i - y_t^i)^2 \quad (6)$$

(2) Graph smoothness constraint on Y . Inspired by the recent work on graph signal processing ([Grassi et al., 2018](#); [Ortega et al., 2018](#); [Shuman et al., 2013](#)), y_t at each time point t can be regarded as a graph signal that resides on the same graph G , where the relationship between any two elements in y_t should follow the context in the latent functional brain network. That is, if there exists a high weight w_{ij} of FC between the nodes v_i and v_j , they should have similar scalar signal value y_t^i and y_t^j , which can be quantified as:

$$\| Y \|_{L_G} = \text{tr}(Y^\top L_G Y) = \sum_{t=1}^T \sum_{ij} w_{ij} (y_t^i - y_t^j)^2 \quad (7)$$

(3) Regularization term on graph Laplacian L_G . In order to guarantee L_G is a valid estimated Laplacian matrix, we regularize the L_G by applying Frobenius norm $\| L_G \|_F^2$ and the trace norm $\text{tr}(L_G) = N$ that equals the number of network nodes N (to avoid the degeneration of solution space).

By combining all the constraints mentioned above, the overall energy function for estimating the dynamic graph Laplacian matrix L_G is:

$$\arg \min_{Y, L_G} \| X - Y \|_F^2 + \mu_1 \| Y \|_{L_G} + \mu_2 \| Y \|_{L_T} + \eta \| L_G \|_F^2, \quad \text{s.t. } \text{tr}(L_G) = N \quad (8)$$

where μ_1 and μ_2 control the strength of graph and temporal smoothness, respectively, and η controls the strength of $\| L_G \|_F^2$.

Since Y and L_G are coupled in Eq. (8), we present an alternative solution to optimize Y and L_G one after another until converging which has been used in our previous work ([Kim et al., 2019](#)). The optimization details are shown step by step in the Supplemental Materials. Since the optimization problem of either Y and L_G is relatively easier, it is efficient to obtain the harmonic-Fourier bases and generate the dynamic graph embedding for each time point described below.

2.4 Dynamic graph embedding

Given the harmonic bases Φ_G from the learned graph Laplacian L_G and the classic Fourier bases Φ_T , we form a dynamic graph J spanned by Φ_G and Φ_T jointly, which has a multi-layer graph structure, as shown in **Fig. 4**. As demonstrated in ([Grassi et al., 2018](#)), the spectrum of dynamic graph J is encoded in the Laplacian matrix L_J as:

$$L_J = L_T \otimes I_G + I_T \otimes L_G \quad (9)$$

where \otimes denotes a Cartesian product. Likewise, the Eigenvector of L_J is the Cartesian product of Φ_G and Φ_T :

$$L_J = (\Phi_T \otimes \Phi_G)(\Lambda_T \otimes I_G + I_T \otimes \Lambda_G)(\Phi_T \otimes \Phi_G)^\top = \Phi_J \Lambda_J \Phi_J^\top \quad (10)$$

Next, we generate the dynamic graph embedding vectors for the BOLD signals in each sliding window. Without loss of generality, the sliding window size is set to P ($P < T$). Then, we partition the entire BOLD signals into S overlapped segments. Each segment becomes a sliding window Ω_s ($s = 1, \dots, S$) with P time points. Furthermore, we use t_s to denote the center of the sliding window Ω_s . As a common practice in signal processing, we truncate the first P Fourier bases in Φ_T and yield the window-specific temporal bases Φ_P . The dynamic graph embedding vector F_s for the sliding window Ω_s can be calculated by:

$$F_s = (\Phi_P \otimes \Phi_G)^\top Y_{\Omega_s} = \Phi_G^\top Y_{\Omega_s} \Phi_P \quad (11)$$

where Y_{Ω_s} denotes the intrinsic BOLD signals within the sliding window Ω_s . The intuition of dynamic graph embedding F_s can be interpreted as (1) dynamic spectral embedding by applying discrete Fourier transform $\hat{Y}_{\Omega_s} = Y_{\Omega_s} \Phi_P$ on the intrinsic BOLD signals, and (2) graph spectral embedding by applying graph Fourier transform $\Phi_G^\top \hat{Y}_{\Omega_s}$.

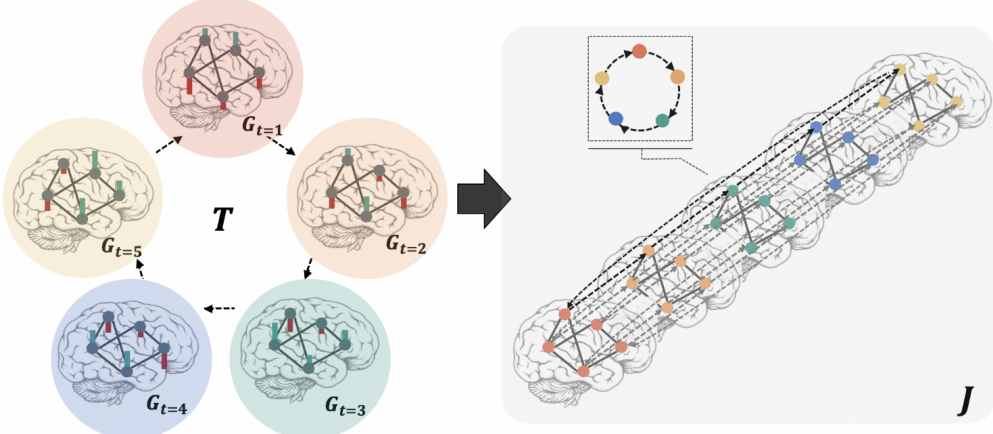


Fig. 4. The dynamic graph J is constructed by the Cartesian product of the graph G and a cyclic graph T in the temporal domain.

2.5 Detect changes in functional connectivity

In dynamic brain network theory, we assume that the FC states are quasi-stationary within a time interval, that is, changes in brain state usually happen between different time intervals. Thus, it is reasonable to cluster the dynamic functional brain network into a number of quasi-stationary brain states. Given the dynamic graph embedding vector F_s at each sliding window, we opt to use a classic spectral clustering method (Ng et al., 2002) to automatically detect the changes of FC. In general, the main steps for detecting changes of FC based on dynamic graph embedding can be summarized as follows: (1) Learn the latent graph Laplacian matrix L_G and estimate the intrinsic BOLD signals Y by optimizing Eq. (8). (2) Construct a joint vertex-time spectrum domain. (3) For each time point t_s , we construct a sliding window Ω_s centered at t_s , and project the intrinsic BOLD signals Y_{Ω_s} to the joint spectrum domain to obtain the dynamic graph embedding vector F_s by Eq. (11). (4)

Based on the embedding vectors $\{F_s\}_{s=1}^S$, the classic spectral clustering is employed to cluster all F_s s into K cognitive states (K is pre-defined). Given the clustering result, the changes in the functional connectivity can be determined by judging the transition of clustering categories along with the time series.

3 Results

In this section, we evaluate the performance of our dynamic graph embedding (dGE) method for detecting changes of FC on both simulated datasets and real fMRI data from HCP (Human Connectome Project) database. Our proposed method is compared with the following two methods: (1) the dynamic brain state tracking method, i.e., sliding window correlation method (SWC) ([Allen et al., 2014](#)) and (2) the simplified version of our proposed method that only utilizes the learned harmonic bases Φ_G , called static graph embedding (sGE) ([Kim et al., 2019](#)). Specifically, the input to SWC method is a set of vectorized functional brain networks constructed within the sliding window, where each sliding window is centered at the underlying time point and uses the same window length as our dGE method. Instead of estimating the FC matrices based on the independent components by group ICA ([Calhoun et al., 2001](#)) as in the original SWC work ([Allen et al., 2014](#)), we construct functional brain networks from BOLD signals directly. Although the feature representations of functional dynamics vary across three change detection methods, all of them use the spectral clustering method ([Ng et al., 2002](#)) to group time points into different cognitive tasks.

We use the grid search strategy to determine the parameters for η (Foubenius norm constraint on Laplacian matrix L_G), μ_1 (graph smoothness constraint), and μ_2 (temporal smoothness constraint), where η ranges from 0.0 to 2.0, and μ_1 and μ_2 range from 0.01 to 1.0. The optimal parameter ranges are found stable where η is around 1.0, μ_1 is around 0.1, and μ_2 is around 0.15. In the following experiments, we fix the parameters to $\eta = 1.0$, $\mu_1 = 0.1$, and $\mu_2 = 0.15$.

3.1 Evaluation of simulated data

3.1.1 Sensitivity analysis on different window sizes

In this experiment, we examine how the selection of window size P affects the detection of FC changes. Since the ground truth is known, we use the clustering purity score ([Manning et al., 2008](#)) to measure the clustering accuracy between the ground truth and automatic detection results. Specifically, we calculate the purity score in the following two steps: (1) for each identified cluster, count the number of time points from the most common task; and (2) take the sum over all clusters and divided by the number of time points. [Fig. 5\(a\)](#) shows the clustering accuracy results by sliding window correlation (in green), static graph embedding (in blue), and our dynamic graph embedding method (in red), where our method consistently achieves the highest accuracy (on average 4.6% higher than SWC and 32.2% higher than sGE) with respect to different window sizes. We note that both the sliding window correlation and our dynamic graph embedding method outperform the static graph embedding method, which does not model the functional dynamics.

3.1.2 Robustness analysis to noise

Here, we study the performance of FC changes detection with respect to different noise levels. To do so, we randomly sample 10% time points from the simulated BOLD signals and add uncorrelated additive Gaussian noise with SNR levels ranging from 5 dB to 50 dB. As shown in **Fig. 5(a)**, the performance of SWC method achieves the highest detection accuracy with window size ranged from 20 to 30 time points. Hence, we set the window size to 22 time points and keep this setting for all methods in the following experiments. The change detection accuracy curves with respect to noise level by sliding window correction, static graph embedding, and our dynamic graph embedding are displayed in green, blue, and red, respectively, in **Fig. 5(b)**. It is clear that our dynamic graph embedding method is much more robust to the noise presented in the BOLD signals than the other two methods (on average 25.1% higher than SWC and 46.0% higher than sGE), which shows the advantage of new feature representations learned from the latent vertex-time domain.

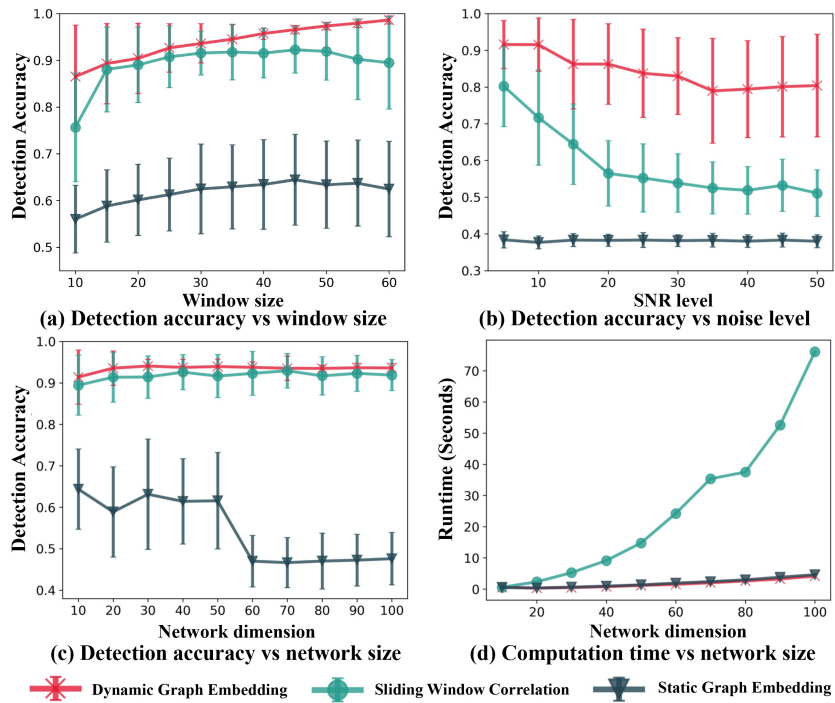


Fig. 5. The performance of the detection of functional connectivity changes on the simulated dataset compared between the sliding window correlation (SWC) method, static graph embedding method (sGE), and our proposed method (dGE), based on (a) effect of window size, (b) noise level, and (c) network size. Besides, we show the computation cost with respect to the number of network nodes in (d).

3.1.3 Scalability in network size

To evaluate the accuracy of change detection as network size increases, we expand the simulated networks generated in Section 3.1.1 from 10×10 to 100×100 . As shown in **Fig. 5(c)**, our dynamic graph embedding method consistently outperforms the other two methods. Note, it is clear that both dGE and SWC methods show less sensitivity to the network size, which can maintain the detection accuracy beyond 0.9 as the network size increases from 10×10 to 100×100 . Since the sGE method does not take functional dynamic information into

account, the detection accuracy drops significantly from 0.6 to less than 0.5 as the network dimension beyond 50 nodes. The computational cost as the number of nodes increases in the network, as shown using computation time in **Fig. 5(d)**. It is apparent that our dGE method (along with sGE) only has a marginal increase of computational cost as the network expands from 10×10 to 100×100 , compared to a large increase in computation time for SWC.

3.2 Application to task-based fMRI data

3.2.1 Detection of functional connectivity changes

In this section, we evaluate the accuracy of change detection using the BOLD signals on 58 nodes in the default mode network (DMN) and attention network (ATN). *First*, we quantitatively evaluate the detection accuracy to different window sizes by varying the window size from 10 to 60 TRs, and showing the mean and standard deviation of purity scores over all 60 task fMRI scans, the detection curves with respect to different window sizes are provided in **Fig.6 (a)**, where our proposed method (in red) consistently outperforms the other two methods (on average 2.1% higher than SWC and 9.3% higher than sGE) in different window sizes. Based on the result, we fix the window size to 22 time points (i.e., 22 TR=15.8 seconds) in the following experiments.

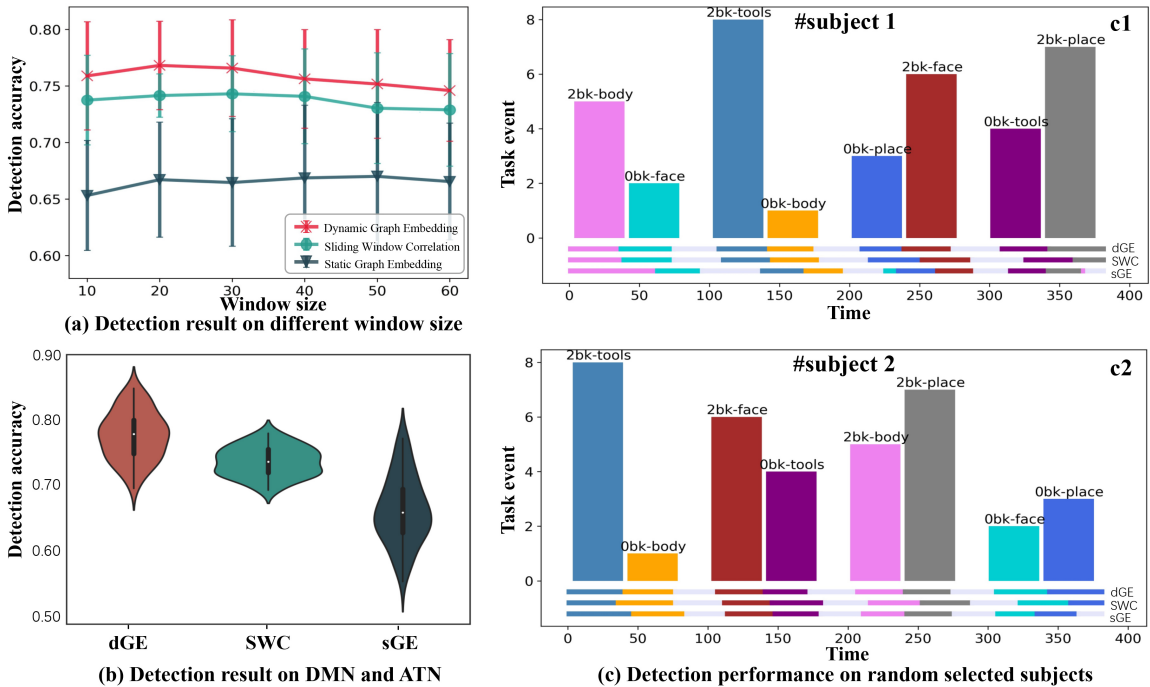


Fig. 6. The performance of detecting FC changes by our dynamic graph embedding method (dGE), with the comparison to the sliding window correlation method (SWC) and static graph embedding method (sGE). (a) The detection accuracy curves with respect to sliding window size by SWC (green), sGE (blue), and our dGE method (red). (b) The average detection accuracy by SWC (green), sGE (blue), and our dGE method (red). (c) The detection performance of our proposed method on two typical task fMRI scans, where the ground truth and automatic detection results are shown in the top and bottom, respectively. Note, the results shown here are based on BOLD signals from 58 nodes in the DMN and ATN.

Second, we show the mean and standard deviation of purity scores over 60 task fMRI scans in **Fig. 6(b)**, where the average purity score is 0.734 by SWC, 0.663 by sGE, and 0.771 by our dGE method. Note, we demonstrate the scalability of our change detection method in Section 3.2.2.

Third, we further demonstrate the FC change detection results of two typical fMRI scans in **Fig. 6(c1-c2)**, where each functional task is designated by bars in different heights. For clarity, we further assign a different color to each task. Note that for these two particular scans, the ordering of the tasks is different. At the bottom of **Fig. 6(c)**, we display the automatic detection results by our dynamic graph embedding method (1st row), sliding window correlation (2nd row), and static graph embedding method (3rd row). Based on the temporal alignment between the pre-defined functional tasks and the automatic detection result, our dynamic graph embedding method has a more accurate prediction than the other two methods.

3.2.2 Scalability of dynamic graph embedding

In this experiment, we evaluate the detection accuracy of change detection methods with respect to different network sizes. To achieve this, we increase the number of network dimensions by successively adding nodes from sub-networks like default mode network (DMN), attention network (ATN), visual network (VIS), and sensorimotor network (SMN) until we cover the whole brain, and evaluate the detection accuracy at different network dimensions. The selected nodes at different network dimensions are shown on the top of **Fig. 7**, and the corresponding detection results are shown in the middle of **Fig. 7**. Our proposed dGE method constantly outperforms the compared methods on different network sizes, where ‘*’ indicates the significant improvement

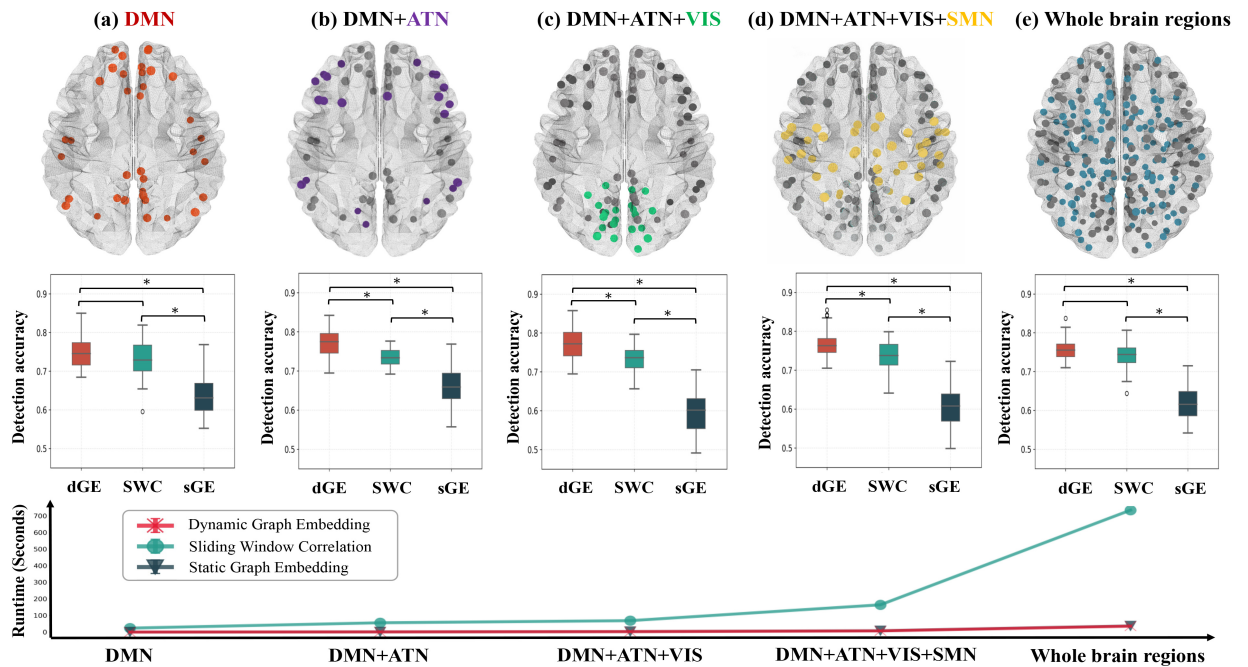


Fig. 7. The detection accuracy (middle) and computational time (bottom) with respect to different network dimensions. From (a)-(d), we show the accuracy and computation time by progressively including ATN, VIS, and SMN to DMN, until the whole brain is covered (e).

using a two-sample t -test ($p < 0.05$). We also show the computation time at the bottom of **Fig. 7** (Note, the curves by dGE and sGE overlap since they have very similar computational time). Similar to the result in **Fig. 5(d)**, our method is more scalable to be deployed to large-scale brain networks than SWC.

3.2.3 Classification of functional task events

In this experiment, we examine the classification performance of our graph embedding vectors in recognizing 2-back task event versus 0-back task event in working memory task-based fMRI data by training a support vector machine (SVM). Although there are four 0-back tasks and four corresponding 2-back tasks in the entire scan, we train four separate binary SVMs to differentiate 0-back/2-back body part tasks, 0-back/2-back place tasks, 0-back/2-back face tasks, and 0-back/2-back tool tasks, respectively. In training each SVM, the dynamic graph embedding vector is considered as the feature vector of the underlying time point, and the associated functional task is used as the label.

We evaluate the task classification results using 10-fold cross-validation for recognizing 0-back/2-back body part tasks, 0-back/2-back place tasks, 0-back/2-back face tasks, and 0-back/2-back tool tasks, respectively. From **Fig. 8(a)-(d)**, we show the ROC (receiver operating characteristics) curves of classifying 2-back task versus 0-back task for body parts, places, faces, and tools by using BOLD signals in sliding window correlation (in green), static graph embedding vectors (in blue), and our dynamic graph embedding vectors (in red), respectively, where x and y axes denote for false positive rate (FPR) and true positive rate (TPR). Note, the ROC curve reflects the TPR against FPR at various thresholding settings. It is clear that the SVM trained by using our dynamic graph embedding vectors achieves the highest classification accuracy in all functional tasks than the SVMs trained using other features.

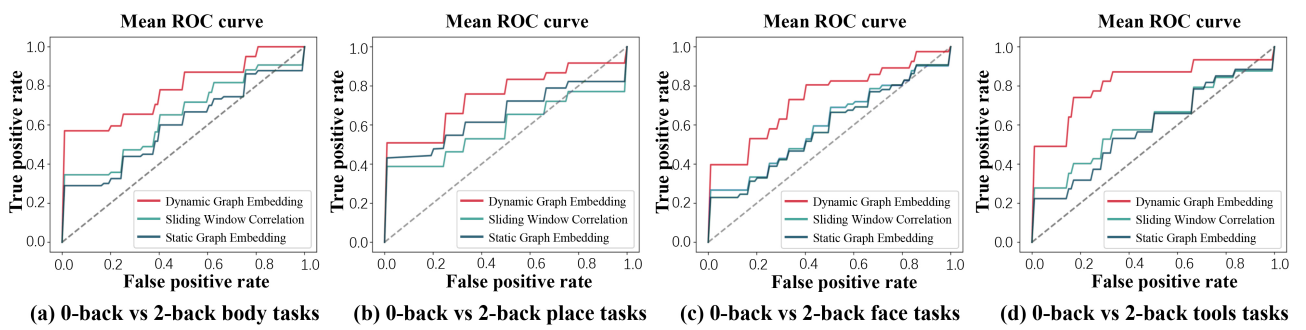


Fig. 8. The ROC curve of 2-back versus 0-back task event classification involving body parts, places, faces, and tools task compared between the three methods.

3.3 Discussion

In both experiments on simulated and real task-based fMRI data, we find that our dynamic graph embedding method achieves significant improvement over the conventional method that directly uses BOLD signals. We propose that the performance gain might come from the graph learning technique and the joint vertex-time domain of dynamic graph embedding vectors. Thus, we first evaluate the contribution of these two

components. After that, we discuss the study limitations and possible application of our dynamic graph embedding method.

Mechanism of joint graph learning and BOLD signals smoothing. Due to the significant amount of external noise in the BOLD signals, feature representations extracted from the original BOLD signals might undermine the detection accuracy. Most current preprocessing methods only use the heuristics in the temporal domain to suppress the noise for each time course separately, ignoring the topological interactions across BOLD signals. Our method can simultaneously remove the external noise (less relevant to the brain activity) in the BOLD signals and optimize the harmonic bases for the vertex-time domain in the graph Laplacian learning process. In **Fig. 9**, we display the BOLD signals (left) of two typical brain regions of interest and the frequency spectrums (right) of the original BOLD signal (black), smoothed BOLD signal utilizing Gaussian filtering (blue), and smoothed BOLD signal by our graph learning method (red). Although the Gaussian smoothing and our graph filtering both use the low-pass filters, our method has more capability to maintain the detail than Gaussian smoothing, as the spectrum curve of harmonic magnitudes (shown in the zoom-in view 3 in **Fig. 9**) by our method is apparently above the spectrum curve by Gaussian smoothing. After visually inspecting the recovered BOLD signals, we found that the smoothing results by both methods are very similar when the BOLD signal is relatively stable. However, our method can maintain much more intrinsic changing patterns (shown in the zoom-in view 1 and 2 in **Fig. 9**) than Gaussian smoothing when BOLD fluctuations occur.

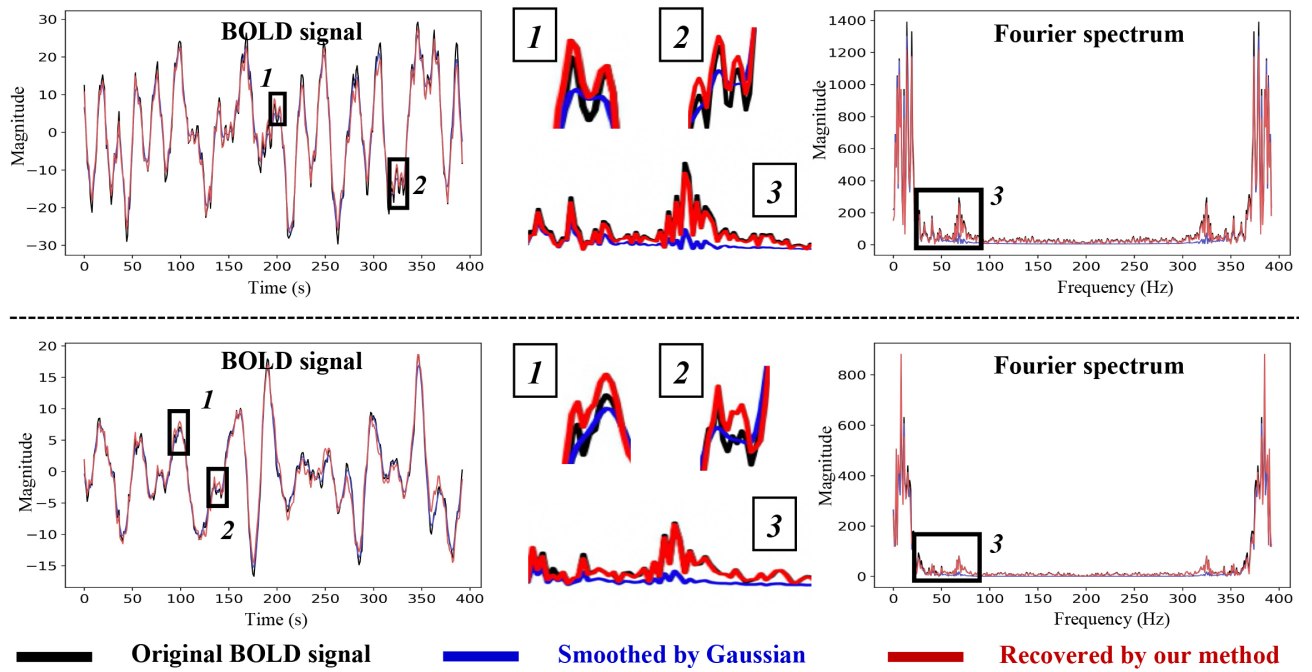


Fig. 9. The BOLD signals (left) and frequency spectrum (right) of the original BOLD signals (black), smoothed BOLD signals by Gaussian filter (blue), and smoothed BOLD signals recovered by our method (red) from two selected brain regions. Furthermore, we zoom in the overlap of BOLD signals in view 1-2 and spectrum in view 3, respectively.

Joint vertex-time domain for capturing the functional dynamics. The spatial-temporal information is highly mixed in the original BOLD signal. Thus, the accurate detection of FC change is indispensable to the disentanglement of functional connectivity and functional dynamics. Our dynamic graph embedding method opts to find the vertex-time domain from the observed BOLD signal. Thus, the resulting dynamic graph embedding vectors have more sensitivity to capture the dynamic changes and characterize the changing patterns. As shown in **Fig. 5** and **Fig. 6**, our novel feature representations show more discriminative power to detect FC changes than conventional methods. Furthermore, we visualize the harmonic basis of two randomly selected subjects in **Fig. 10**. In the left top panel of **Fig. 10**, we display in total 268 brain parcellations on the cortical surface, where the colormap down below shows the assigned color for the nodes in default mode network, attention network, dorsal attention network, sensorimotor network, salience network, basal ganglia network, visual network, respectively. Next, we shuffle the elements in each harmonic basis and plot the signals in a module-by-module manner, where color indicates the associated sub-network. Furthermore, in the left bottom panel, we display 10 randomly selected brain regions, and plot the signals on each brain region. Here, we only show the harmonic bases representing the low, middle, and high-frequency bands. In general, low-frequency harmonic bases exhibit slow waves all over the brain. On the contrary, high-frequency counterparts show the pattern of localized rapid fluctuations.

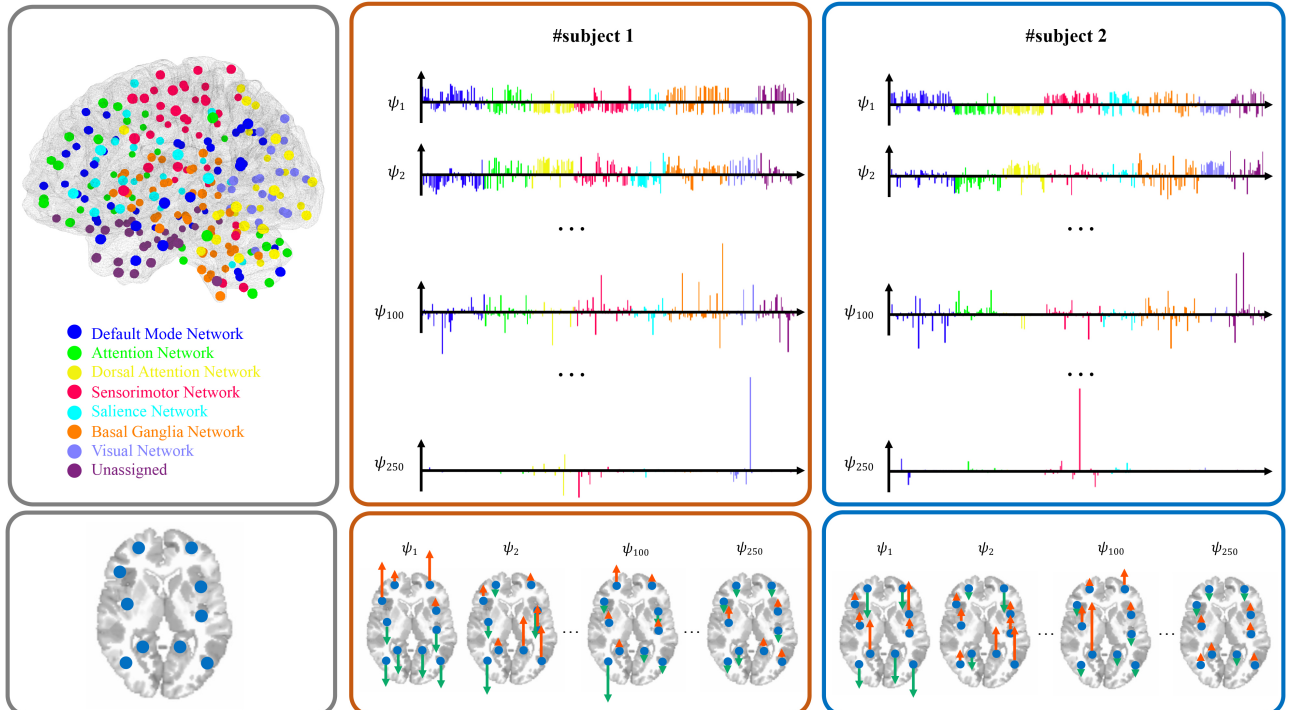


Fig. 10. Top: (1) left: 268 brain parcellations on the cortical surface, where the color indicates the sub-networks. (2) middle and right: from top to bottom, we plot the low, middle, and high harmonic bases for two subjects, where color indicates the associated sub-networks; Bottom: (1) left: 10 brain regions on the brain slice. (2) middle and right: from left to right, we plot the low, middle, and high harmonic bases on each brain region for the two subjects.

Limitations of our dynamic graph embedding and possible solutions. The goal of our graph-based learning approach is to generate a new embedding vector that can describe the functional dynamics at each time. However, our current method has several limitations. *First*, given the global nature of our harmonic-Fourier bases, our method does not readily lend itself to mapping the frequency-based bases to the brain and identifying the task-relevant brain regions. One possible solution is to localize the harmonic-Fourier bases using a post-hoc optimization methods ([Melzi et al., 2018](#)) which have been studied in the shape analysis area. *Second*, our current graph learning approach is unsupervised, which is steered by the temporal characteristics of the BOLD signals and network topology, instead of cognitive tasks. For the possible application of recognizing functional tasks (such as in Section 3.2.3), supervised feature representation learning or feature selection is needed to make the features more discriminative across tasks. *Third*, since we apply our graph learning approach to each subject separately, the resulting harmonic-Fourier bases are subject-specific. Thus, it is hard to find common task-relevant patterns across individuals. Recently, we have developed a manifold-based learning method to unify the harmonic bases on the Stiefel manifold ([Chen et al., 2020](#)), which can be used to find common harmonic-Fourier bases of functional brain networks for group comparison studies.

Relevant works and future direction. In our previous work ([Bahrami et al., 2019](#)), we were interested in investigating the across-task relationships between dynamic brain networks by projecting the FC matrices into a low-dimensional space. However, the feature representation that can characterize the underlying functional dynamic was not the focus of this proof-of-concept work. Similarly, the study in ([Shine et al., 2018](#)) investigated context-sensitive balance between functional integration and segregation in the brain by examining the temporal trajectories of network properties such as participation coefficients and modularity degree ([Rubinov and Sporns, 2010](#)). Since our harmonic-like bases offer a new feature representation to capture the functional dynamics with a greater insight into mathematics and network neuroscience, our future work includes (1) applying the dynamic graph embeddings to identify task-specific fingerprints that can discriminate cognitive tasks across individuals, and (2) understanding the functional dynamics using the well-studied physics concepts such as power and energy.

4 Conclusion

In this paper, we develop a novel learning-based approach to detect changes in functional connectivity. Our dynamic graph embedding learning method is designed to amplify the sensitivity to capture the cognitive changes from fMRI data. The backbone of our method is a graph learning approach, which allows us to characterize the intrinsic functional connectivity at each time point and capture functional fluctuations during the scan. The outcome of our method is a set of novel putative dynamic graph embeddings, which can be used to identify the change points by clustering the dynamic graph embeddings into temporal segments. Promising results have been found on both simulated data and real task fMRI datasets, which indicate the great potential of our dynamic graph learning approach in the neuroscience field.

Supplemental material

To solve the optimization problem in Eq. (8), we present the following optimization approach with the following two steps.

Step1: Smooth signals by joint filtering. By fixing the dynamic Laplacian L_T and graph Laplacian L_G , the energy function of estimating the intrinsic clean signals Y becomes:

$$\arg \min_Y \|X - Y\|_F^2 + \mu_1 \text{tr}(Y^\top L_G Y) + \mu_2 \text{tr}(Y^\top L_T Y) \quad (12)$$

Since Eq. (12) is a classic Tikhonov regularization problem ([Shuman et al., 2013](#)), we have the following closed-form solution for \hat{Y} :

$$\text{vec}(\hat{Y}) = (\mu_1 L_T \otimes I_G + \mu_2 I_T \otimes L_G + I)^{-1} \text{vec}(X) \quad (13)$$

where \otimes is the Kronecker product operator. In graph spectrum theory ([Shuman et al., 2013](#)), the main intuition of Eq. (13) can be interpreted as filtering the observed BOLD signals X by the graph spectrum domain encoded in L_G and the temporal domain encoded in L_T . For instance, the fluctuation pattern along the temporal domain can be analyzed by using the Discrete Fourier transform (DFT) to each row of X :

$$DFT(X) = X\Phi_T \quad (14)$$

Similarly, the graph Fourier transform (GFT) can be utilized on each column of X to analyze the fluctuation pattern along the graph spectrum domain:

$$GFT(X) = \Phi_G^\top X \quad (15)$$

where $\Phi_G(n)$ is the eigenvector of L_G with the corresponding eigenvalue $\lambda_G(n)$. Thus, filtering BOLD signals X by a joint filter h can be equivalently seen as:

$$\text{vec}(\hat{Y}) = h(L_G, L_T) \text{vec}(X) = \sum_{n=1,t=1}^{N,T} \Phi_J h(\lambda_G(n), \lambda_T(t)) \Phi_J^\top \text{vec}(X) \quad (16)$$

$$h(\lambda_G(n), \lambda_T(t)) = \frac{1}{1 + \mu_1 \lambda_T(t) + \mu_2 \lambda_G(n)} \quad (17)$$

where $\Phi_J = \Phi_T \otimes \Phi_G$ represents the joint harmonic-Fourier bases of the smoothing kernel h . As shown in Eq. (17), h is a low-pass filter that attenuates high-frequency component more aggressively than low-frequency component, and larger values of μ_1 and μ_2 result in smoother BOLD signals along the temporal and graph domains.

Step 2: Estimate the dynamic graph Laplacian. By fixing Y , the optimization of L_G can be done by minimizing $\mu_1 \|Y\|_{L_G} + \eta \|L_G\|_F^2$. Since the range of each element in the adjacency matrix W is fixed, we resort to a relatively easier optimization scenario by searching for an adjacency matrix W instead of L_G ([Kalofolias, 2016](#)), where minimizing $\|L_G\|_F^2$ is equivalent to minimizing the term $(\|W\|_F^2 + \|W\mathbf{1}\|_2^2)$. Then the equivalent energy function is obtained as:

$$\arg \min_W \text{tr}(Y^\top W Y) + \sigma \|W\|_F^2 + \sigma \|W\mathbf{1}\|_2^2, \quad s.t. \quad \|W\mathbf{1}\|_1^2 = N \quad (18)$$

where $\sigma = \frac{\eta}{\mu_1}$ controls the sparsity of W . Note that for $\sigma = 0$, we have a very sparse solution that assigns weights to the edge corresponding to the smallest pairwise distance in $Y^T W Y$ and zero everywhere else. On the other hand, we intend to penalize large degrees in the node degree vector $W\mathbf{1}$ by setting σ to big values. In the limit $\sigma \rightarrow \infty$, we obtain a dense adjacency matrix W with a constant degree. The constraint of each row-wise summation equals to the total number of graph nodes ($\|W\mathbf{1}\|_1^1 = N$) is used to avoid the degenerative solution. This objective function can be solved in the classic ADMM (Alternating Direction Method of Multipliers) framework (Boyd et al., 2011). The objective function in Eq. (18) can be first transformed into the following equation:

$$\arg \min_{w_i} w_i d_i + \sigma \mathbf{1}^\top w_i^\top w_i \mathbf{1} + \sigma w_i w_i^\top, \quad s.t. \quad \sum_{i=1}^n w_i \mathbf{1} = N, w_i \geq \mathbf{0} \quad (19)$$

where $d_i = [d_{ij}]_{j=1,2,\dots,N} = [(y_t^i - y_t^j)^2]_{j=1,2,\dots,N} \in R^{N \times 1}$ is a column vector and $w_i \geq \mathbf{0}$ means that a positive or zero correlation between region i and region j ($w_{ij} \geq 0$) can be regarded as effective functional connectivity. Then, the Lagrangian function of Eq. (19) can be obtained:

$$w_i d_i + \sigma \mathbf{1}^\top w_i^\top w_i \mathbf{1} + \sigma w_i w_i^\top - \xi (\sum_{i=1}^n w_i \mathbf{1} - N) - w_i \beta_i \quad (20)$$

where $\xi \geq 0$ and $\beta_i \geq \mathbf{0}$ are the Lagrange multipliers that combine the objective function and constraints together. Based on the mathematical optimization about KKT conditions (Boyd et al., 2004), we can get the following equation:

$$\begin{cases} d_i^\top + 2\sigma w_i + 2\sigma w_i (\mathbf{1} \cdot \mathbf{1}^\top) - \xi \mathbf{1}^\top - \beta_i^\top = 0 \\ w_i \geq \mathbf{0} \\ w_i \beta_i = 0 \\ \beta_i \geq \mathbf{0} \end{cases} \quad (21)$$

According to the complementary slackness KKT condition, we must ensure that β_i is equal to $\mathbf{0}$ when $w_i \geq \mathbf{0}$, thus we have:

$$w_i = \frac{1}{2\sigma(N+1)} [\xi - (N+1)d_i^\top + d_i^\top \mathbf{1} \cdot \mathbf{1}^\top] \quad (22)$$

Given the constraint $w_i \geq \mathbf{0}$, we can transform Eq. (22) into:

$$w_{ij} = \left(\frac{1}{2\sigma(N+1)} [\xi - (N+1)d_{ij} + \sum_{j=1}^N d_{ij}] \right)_+ \quad (23)$$

where $(a)_+ = \max(0, a)$ is the positive part of the variable a .

Thus, the estimation of parameter ξ can be solved as below. Supposing that $d_{i1}, d_{i2}, \dots, d_{iN}$ are ordered in an ascent manner like the Lemma 1 in (Duchi et al., 2008), we can choose l non-zero elements in the optimal w_i by letting $w_{il} > 0$ and $w_{i,l+1} = 0$.

$$\begin{cases} \frac{1}{2\sigma(N+1)} [\xi - (N+1)d_{il} + \sum_{j=1}^N d_{ij}] > 0 \\ \frac{1}{2\sigma(N+1)} [\xi - (N+1)d_{i,l+1} + \sum_{j=1}^N d_{ij}] \leq 0 \end{cases} \quad (24)$$

Furthermore, together with the constraint $\sum_{i=1}^n w_i \mathbf{1} = N$, we have the value of ξ :

$$\xi = \frac{2\sigma(N+1)}{K} + \left(\frac{N+1}{KN} \right) \sum_{i=1}^N \sum_{j=1}^l d_{ij} - \frac{1}{N} \sum_{i,j=1}^N d_{ij} \quad (25)$$

After solving w_i for each row i , we can get the adjacency matrix W .

Table 1. List of nodes refer to default mode network and attention network in the Shen. Atlas.

	ID	Region name (Brodmann area)		ID	Region name (Brodmann area)
Default Mode Network	3	R.BA11	Attention Network	7	R.BA10
	5	R.BA10		8	R.BA10
	6	R.BA10		11	R.BA9
	10	R.BA9		14	R.BA8
	12	R.BA8		19	R.BA46
	13	R.BA8		22	R.BA44
	48	R.BA39		30	R.BA6
	50	R.BA39		47	R.BA40
	55	R.BA21		70	Fusiform(37)
	56	R.BA20		111	Cerebellum
	64	R.BA22		112	Cerebellum
	85	R.BA23		142	L.BA10
	86	R.BA23		143	L.BA10
	90	R.BA31		147	L.BA9
	100	Cerebellum		149	L.BA8
	134	L.BA11		150	L.BA8
	137	L.BA11		154	L.BA46
	138	L.BA10		156	L.BA44
	140	L.BA10		157	L.BA6
	141	L.BA10		184	L.BA39
	145	L.BA9		199	Fusiform(37)
	146	L.BA9		246	Cerebellum
	148	L.BA8			
	176	L.BA7			
	182	L.BA39			
	183	L.BA39			
	187	L.BA38			
	190	L.BA21			
	193	L.BA21			
	196	L.BA20			
	222	L.BA23			
	223	L.BA23			
	225	L.BA31			
	227	L.BA30			
	239	Cerebellum			
	242	Cerebellum			

References

- Allen, E., Damaraju, E., Eichele, T., Wu, L., Calhoun, V.D., 2018. EEG signatures of dynamic functional network connectivity states. *Brain topography* 31, 101-116.
- Allen, E.A., Damaraju, E., Plis, S.M., Erhardt, E.B., Eichele, T., Calhoun, V.D., 2014. Tracking whole-brain connectivity dynamics in the resting state. *Cerebral cortex* 24, 663-676.
- Bahrami, M., Lyday, R.G., Casanova, R., Burdette, J.H., Simpson, S.L., Laurienti, P.J., 2019. Using Low-Dimensional Manifolds to Map Relationships Between Dynamic Brain Networks. *Frontiers in Human Neuroscience* 13.
- Bastos, A.M., Schoffelen, J.-M., 2016. A tutorial review of functional connectivity analysis methods and their interpretational pitfalls. *Frontiers in systems neuroscience* 9, 175.
- Biswal, B., Zerrin Yetkin, F., Haughton, V.M., Hyde, J.S., 1995. Functional connectivity in the motor cortex of resting human brain using echo-planar MRI. *Magnetic resonance in medicine* 34, 537-541.
- Boyd, S., Boyd, S.P., Vandenberghe, L., 2004. Convex optimization. Cambridge university press.
- Boyd, S., Parikh, N., Chu, E., Peleato, B., Eckstein, J., 2011. Distributed optimization and statistical learning via the alternating direction method of multipliers. *Foundations and Trends® in Machine learning* 3, 1-122.
- Calhoun, V.D., Adali, T., Pearlson, G.D., Pekar, J.J., 2001. A method for making group inferences from functional MRI data using independent component analysis. *Human Brain Mapping* 14, 140-151.
- Calhoun, V.D., Miller, R., Pearlson, G., Adali, T., 2014. The chronnectome: time-varying connectivity networks as the next frontier in fMRI data discovery. *Neuron* 84, 262-274.
- Chen, J., Han, G., Cai, H., Yang, D., Laurienti, P.J., Styner, M., Wu, G., 2020. Learning Common Harmonic Waves on Stiefel Manifold - A New Mathematical Approach for Brain Network Analyses. *IEEE Trans Med Imaging* Pp.
- Cline, A.K., Dhillon, I.S., 2006. Computation of the singular value decomposition.
- Cribben, I., Haraldsdottir, R., Atlas, L.Y., Wager, T.D., Lindquist, M.A., 2012. Dynamic connectivity regression: determining state-related changes in brain connectivity. *Neuroimage* 61, 907-920.

Damaraju, E., Allen, E.A., Belger, A., Ford, J.M., McEwen, S., Mathalon, D., Mueller, B., Pearlson, G., Potkin, S., Preda, A., 2014. Dynamic functional connectivity analysis reveals transient states of dysconnectivity in schizophrenia. *NeuroImage: Clinical* 5, 298-308.

Duchi, J., Shalev-Shwartz, S., Singer, Y., Chandra, T., 2008. Efficient projections onto the l 1-ball for learning in high dimensions, *Proceedings of the 25th international conference on Machine learning*, pp. 272-279.

Erhardt, E.B., Allen, E.A., Wei, Y., Eichele, T., Calhoun, V.D., 2012. SimTB, a simulation toolbox for fMRI data under a model of spatiotemporal separability. *Neuroimage* 59, 4160-4167.

Friston, K.J., 2011. Functional and effective connectivity: a review. *Brain connectivity* 1, 13-36.

Glasser, M.F., Sotiropoulos, S.N., Wilson, J.A., Coalson, T.S., Fischl, B., Andersson, J.L., Xu, J., Jbabdi, S., Webster, M., Polimeni, J.R., 2013. The minimal preprocessing pipelines for the Human Connectome Project. *Neuroimage* 80, 105-124.

Gonzalez-Castillo, J., Bandettini, P.A., 2018. Task-based dynamic functional connectivity: Recent findings and open questions. *Neuroimage* 180, 526-533.

Grassi, F., Loukas, A., Perraudin, N., Ricaud, B., 2018. A Time-Vertex Signal Processing Framework: Scalable Processing and Meaningful Representations for Time-Series on Graphs. *IEEE Transactions on Signal Processing* 66, 817-829.

Gu, S., Pasqualetti, F., Cieslak, M., Telesford, Q.K., Yu, A.B., Kahn, A.E., Medaglia, J.D., Vettel, J.M., Miller, M.B., Grafton, S.T., Bassett, D.S., 2015. Controllability of structural brain networks. *Nature Communications* 6, 8414.

Hindriks, R., Adhikari, M.H., Murayama, Y., Ganzetti, M., Mantini, D., Logothetis, N.K., Deco, G., 2016. Can sliding-window correlations reveal dynamic functional connectivity in resting-state fMRI? *Neuroimage* 127, 242-256.

Honey, C.J., Sporns, O., Cammoun, L., Gigandet, X., Thiran, J.P., Meuli, R., Hagmann, P., 2009. Predicting human resting-state functional connectivity from structural connectivity. *Proceedings of the National Academy of Sciences* 106, 2035.

Hutchison, R.M., Womelsdorf, T., Allen, E.A., Bandettini, P.A., Calhoun, V.D., Corbetta, M., Della Penna, S., Duyn, J.H., Glover, G.H., Gonzalez-Castillo, J., 2013. Dynamic functional connectivity: promise, issues, and interpretations. *Neuroimage* 80, 360-378.

Kalofolias, V., 2016. How to learn a graph from smooth signals.

Kim, M., Moussa, A., Liang, P., Kaufer, D., Laurienti, P., Wu, G., 2019. Revealing Functional Connectivity by Learning Graph Laplacian, 22nd International Conference on Medical Image Computing and Computer Assisted Intervention (MICCAI), Shenzhen, China.

Krüger, G., Glover, G.H., 2001. Physiological noise in oxygenation-sensitive magnetic resonance imaging. Magnetic Resonance in Medicine: An Official Journal of the International Society for Magnetic Resonance in Medicine 46, 631-637.

Lee, H., Kang, H., Chung, M.K., Kim, B.N., Lee, D.S., 2012. Persistent brain network homology from the perspective of dendrogram. IEEE Trans. on Medical Imaging 31, 2267-2277.

Manning, C.D., Raghavan, P., Schütze, H., 2008. Introduction to Information Retrieval. Cambridge University Press.

Medaglia, J.D., Pasqualetti, F., Hamilton, R.H., Thompson-Schill, S.L., Bassett, D.S., 2017. Brain and cognitive reserve: Translation via network control theory. Neuroscience and biobehavioral reviews 75, 53-64.

Melzi, S., Rodolà, E., Castellani, U., Bronstein, M.M., 2018. Localized Manifold Harmonics for Spectral Shape Analysis. Computer Graphics Forum 37, 20-34.

Ng, A.Y., Jordan, M.I., Weiss, Y., 2002. On spectral clustering: Analysis and an algorithm, Advances in neural information processing systems, pp. 849-856.

Ortega, A., Frossard, P., Kovačević, J., Moura, J.M.F., Vandergheynst, P., 2018. Graph Signal Processing: Overview, Challenges, and Applications. Proceedings of the IEEE 106, 808-828.

Pruim, R.H., Mennes, M., van Rooij, D., Llera, A., Buitelaar, J.K., Beckmann, C.F., 2015. ICA-AROMA: A robust ICA-based strategy for removing motion artifacts from fMRI data. Neuroimage 112, 267-277.

Rashid, B., Damaraju, E., Pearlson, G.D., Calhoun, V.D., 2014. Dynamic connectivity states estimated from resting fMRI Identify differences among Schizophrenia, bipolar disorder, and healthy control subjects. Frontiers in human neuroscience 8, 897.

Rubinov, M., Sporns, O., 2010. Complex network measures of brain connectivity: uses and interpretations. NeuroImage 52, 1059-1069.

Schröder, A.L., Ombao, H., 2019. FreSpeD: Frequency-specific change-point detection in epileptic seizure multi-channel EEG data. *Journal of the American Statistical Association* 114, 115-128.

Shakil, S., Lee, C.-H., Keilholz, S.D., 2016. Evaluation of sliding window correlation performance for characterizing dynamic functional connectivity and brain states. *Neuroimage* 133, 111-128.

Shen, X., Tokoglu, F., Papademetris, X., Constable, R.T., 2013. Groupwise whole-brain parcellation from resting-state fMRI data for network node identification. *Neuroimage* 82, 403-415.

Shine, J.M., Aburn, M.J., Breakspear, M., Poldrack, R.A., 2018. The modulation of neural gain facilitates a transition between functional segregation and integration in the brain. *eLife* 7.

Shine, J.M., Koyejo, O., Bell, P.T., Gorgolewski, K.J., Gilat, M., Poldrack, R.A., 2015. Estimation of dynamic functional connectivity using Multiplication of Temporal Derivatives. *NeuroImage* 122, 399-407.

Shuman, D.I., Narang, S.K., Frossard, P., Ortega, A., Vandergheynst, P., 2013. The emerging field of signal processing on graphs: Extending high-dimensional data analysis to networks and other irregular domains. *IEEE Signal Processing Magazine* 30, 83-98.

Sporns, O., 2011. Networks of the brain. MIT Press.

Sporns, O., Chialvo, D.R., Kaiser, M., Hilgetag, C.C., 2004. Organization, development and function of complex brain networks. *Trends in cognitive sciences* 8, 418-425.

Stam, C.J., Nolte, G., Daffertshofer, A., 2007. Phase lag index: assessment of functional connectivity from multi channel EEG and MEG with diminished bias from common sources. *Human brain mapping* 28, 1178-1193.

Van Den Heuvel, M.P., Pol, H.E.H., 2010. Exploring the brain network: a review on resting-state fMRI functional connectivity. *European neuropsychopharmacology* 20, 519-534.

Van Essen, D.C., Smith, S.M., Barch, D.M., Behrens, T.E., Yacoub, E., Ugurbil, K., Consortium, W.-M.H., 2013. The WU-Minn human connectome project: an overview. *Neuroimage* 80, 62-79.

Xu, Y., Lindquist, M.A., 2015. Dynamic connectivity detection: an algorithm for determining functional connectivity change points in fMRI data. *Frontiers in neuroscience* 9, 285.